Cretinism and Loss of Thyroidal Iodide Organification in Mice Deficient in Dual Oxidase Maturation Factors

Abbreviated Title: Cretinism in *Duoxa* deficient mice

Helmut Grasberger[1,2], Xavier De Deken[4], Olga Barca Mayo[2], Houssam Raad[4], Mia Weiss[2], Xiao-Hui Liao[2], Samuel Refetoff[2,3]

[(1)] Departments of Medicine, University of Michigan, Ann Arbor, MI
[(2)] Department of Medicine, [(3)] Pediatrics and Genetics, University of Chicago, IL
[(4)] IRIBHM, Université Libre de Bruxelles, Brussels, Belgium

Correspondence and reprint requests:
Helmut Grasberger
University of Michigan
BSRB, Rm2468
109 Zina Pitcher Place
Ann Arbor, MI 48109
Phone: +1-734-936-6363
Fax: +1-734-763-4686
hgrasber@gmail.com

Keywords:
hypothyroidism, mouse model, dual oxidase, NADPH oxidase

Grant support:
Supported by a Young Investigator Research Grant from the American Thyroid Association (H.G.), the "Fonds National de la Recherche Scientifique" (F.R.S-FNRS) (X.D.D.), …

Disclosure summary:
The authors have nothing to disclose.

ABSTRACT (<= 250)

Dual oxidases (DUOX1 and DUOX2) are evolutionary conserved NADPH oxidases responsible for regulated hydrogen peroxide (H_2O_2) release of epithelial cells. Specific maturation factors (DUOXA1 and DUOXA2) are required for targeting of functional DUOX enzymes to the cell surface. Mutations in the single-copy *Duox* and *Duoxa* genes of invertebrates cause developmental defects with reduced survival, whereas knockdown in later life impairs intestinal epithelial immune homeostasis. In humans, mutations in both *DUOX2* and *DUOXA2* can cause congenital hypothyroidism with partial iodide organification defects compatible with a role of DUOX2-generated H_2O_2 in driving thyroid peroxidase activity. The DUOX1/DUOXA1 system may account for residual iodide organification in patients with loss of DUOX2, but its physiological function is less clear. To provide a murine model recapitulating complete DUOX deficiency, we simultaneously targeted both *Duoxa* genes by homologous recombination. Knockout of *Duoxa* genes (*Duoxa*$^{-/-}$ mice) lead to a maturation defect of DUOX proteins lacking Golgi processing of N-glycans and to loss of H_2O_2 release from thyroid tissue. Postnatally, *Duoxa*$^{-/-}$ mice developed severe goitreous congenital hypothyroidism (cretinism) with undetectable serum T4 and maximally disinhibited TSH levels. Heterozygous mice had normal thyroid function parameters. ^{125}I tracer studies and probing of iodinated TG epitopes corroborated the total iodide organification defect in *Duoxa*$^{-/-}$ mice. *Duoxa*$^{-/-}$ mice on continuous T4 replacement from P6 showed normal growth without an overt phenotype. Our results confirm *in vivo* the requirement of DUOXA for functional expression of DUOX-based NADPH oxidases and the role of DUOX isoenzymes as sole source of hormonogenic H_2O_2. *Duoxa*$^{-/-}$ mice rescued by thyroid hormone replacement can serve as complete DUOX-deficiency model to explore the role of DUOX in extrathyroidal organs.

INTRODUCTION

The central steps in thyroid hormone synthesis take place at the apical membrane of follicular thyroid cells. In the first step, iodide is oxidized and covalently linked to tyrosines of thyroglobulin (TG). In the second step, iodinated tyrosyl residues are linked via an ether bond to iodothyronines (thyroxine [T4] and, to lesser degree, triiodothyronine [T3] and reverse T3). Both reactions are catalyzed by thyroid peroxidase (TPO), the activity of which is controlled by the supply of hydrogen peroxide as final electron acceptor.

The catalytic core of this thyroidal H_2O_2 generator is provided by dual oxidases (DUOX1 and DUOX2; originally called thyroid oxidases or THOX), members of the NOX/DUOX family of NADPH oxidases (1, 2). Their intrinsic activity is acutely stimulated by cytosolic Ca^{2+} and PKC-mediated phosphorylation *in vitro* (3) consistent with the regulation of H_2O_2 production and iodination in thyroid tissue (4, 5).

In heterologous systems, reconstitution of a DUOX-based H_2O_2 generator requires the formation of a heterodimeric complex of DUOX with another multipass transmembrane protein called dual oxidase maturation factor (DUOXA1 and DUOXA2 paralogs) (6). The evolutionary conserved genetic linkage of *DUOX1*/*DUOXA1* and *DUOX2*/*DUOXA2* into transcriptional units provides the basis for strict co-expression of each *DUOX* with the corresponding maturation factor (6-8). Only DUOX1/DUOXA1 and DUOX2/DUOXA2 complexes appear to be fully functional *in vitro* (9, 10).

The DUOX2-based enzyme appears to be most critical for maintaining normal thyroid function, since only mutations in *DUOX2* and *DUOXA2*, but not *DUOX1* or *DUOXA1* genes, have been identified as cause of dyshormonogenesis in patients with congenital hypothyroidism (CH) (reviewed in (11)), and mice deficient in *Duox2* (12), but not *Duox1* (13), are hypothyroid. On the other hand, patients with biallelic, complete loss-of-function *DUOX2* mutations manifest only partial iodide organification defects and sometimes merely hyperthyrotropinemia with normal thyroid hormone levels (compensated hypothyroidism). These data suggest that other sources of H_2O_2, presumably DUOX1, can partially compensate for DUOX2 deficiency.

In evolutionary terms, the adaptation of the DUOX system as driver of TPO activity appears to be a rather recent addition to the functional repertoire of DUOX. DUOX/DUOXA are expressed outside the thyroid, particularly in barrier epithelia, and homologs are present in invertebrates lacking a follicular thyroid or an endostyle thyroid equivalent. For instance, high basal and pathogen-inducible DUOX/DUOXA expression in the epithelium of the gastrointestinal-tract has been conserved from invertebrates, such as, nematodes and fruitfly to mammals including human (14-17). Gene knockdown studies in invertebrate model systems have convincingly demonstrated a crucial function of DUOX-derived H_2O_2 in host-microbial interaction and barrier defense of the intestinal mucosa. Whether the vertebrate DUOX enzymes play a similar role in epithelial innate immunity remains to be investigated in suitable *in vivo* model systems. Furthermore, loss-of-function mutations of the single-copy invertebrate *Duox* and *Duoxa* genes have been associated with severe, frequently lethal developmental abnormalities (14, 15, 18, 19). Up till now, however, no equivalent complete DUOX deficiency model has been generated in higher vertebrates expressing two DUOX isoenzymes.

Here, we introduce a novel mouse model generated by simultaneous targeting of the contiguous *Duoxa* genes (*Duoxa*$^{-/-}$ mice). Our results indicate that DUOXA deficiency in Duoxa$^{-/-}$ mice leads to intracellular retention of the DUOX subunits concomitant with a loss of Ca^{2+}-inducible H_2O_2 release. Loss of DUOX activity in *Duoxa*$^{-/-}$ mice did not affect intrauterine survival or cause apparent inborn developmental defects. However, due to complete lack of thyroidal iodide organification they develop the hallmarks of severe primary congenital hypothyroidism (cretinism) in postnatal life. *Duoxa*$^{-/-}$ mice on continuous postnatal T4 replacement did not display an overt phenotype and, thus, could serve as useful model to explore the function of DUOX-generated H_2O_2 in stress responses of extrathyroidal tissues *in vivo*.

RESULTS

Targeting of *Duoxa1* and *Duoxa2* in embryonic stem cells

The arrangement of the *Duoxa* genes and their relative position to the *Duox* genes is schematically depicted in Fig. 1A. The simultaneous targeting of both *Duoxa* genes was achieved by deletion of a ~2.9 kbp region extending from coding exon 5 of *Duoxa2* to coding exon 5 of *Duoxa1*. Termination of translation at the breakpoints was ensured by the insertion of stop codons (TAG) in the reading frames of the *Duoxa* genes. The resulting truncation of the *Duoxa* coding regions prevents expression of stable, functional proteins (9). Homologous recombination with the targeting vector (Fig. 1A) replaced this region with a self-excising ACN cassette (20). The ACN cassette is flanked with loxP sites and contains the neomycin resistance (*Neo*^{R}) gene under control of the mouse RNA Pol II promoter, together with *Cre* recombinase under the control of the testis-specific promoter of angiotensin-converting enzyme (*tACE*). In addition, a diphtheria toxin subunit A cassette (DTA) was used for negative selection against non-homologous recombination. The final construct was confirmed by restriction digestions and bidirectional sequencing, linearized with *Pme*I and electroporated into feeder-less 129S6 ES cells. Of a total of 144 *Neo*^{R} positive clones, nine were identified that were correctly targeted by homologous recombination as confirmed by long-range PCR assays and Southern blotting (Fig. S1).

Generation of *Duoxa*$^{-/-}$ mice as a model for complete deficiency of both DUOX isoenzymes

Of the correctly targeted ES cell clones, five were injected into C57BL/6J blastocysts at the University of Chicago Transgenic Core Facility. High percentage male chimeras were tested for germline transmission by mating with C57BL/6J WT females. Heterozygous F1 transgenic mice were identified by coat color (agouti) and confirmed by genotyping (Fig. 1B). Note that in ES-cell derived germ cells of chimeric mice, CRE expression lead to self-excision of the ACN cassette during spermatogenesis, with only a single loxP element (flanked by stop codons) remaining in the knockout allele. Except where indicated otherwise, all mice used in this study were F2 hybrid animals, produced by intercrosses of F1 heterozygotes originating

from a single ES cell clone (clone 43). The phenotype of *Duoxa*$^{-/-}$ mice described below was confirmed in a smaller number of knockout animals derived from two additional ES cell clones.

Duoxa$^{-/-}$ mice express detectable amounts of mRNA from the truncated *Duoxa* loci as determined by RT-PCR with PCR primers upstream of the introduced stop codons (Fig. 1C, D). 3'RACE-PCRs did not result in a specific product for the truncated *Duoxa1* locus (Δ*Duoxa1*) locus, but identified a stable, polyadenylated Δ*Duoxa2* transcript that contained the in-frame stop codon as expected (Fig. S2). Expression of *Duox1* and *Duox2* were similar between *Duoxa*$^{-/-}$ and WT mice in extrathyroidal tissues suggesting that the targeting did not disrupt *cis* elements crucial for *Duox* gene expression. In contrast, but compatible with the relatively high level of the polyadenylated Δ*Duoxa2* mRNA in the thyroid of *Duoxa*$^{-/-}$ mice, expression of both *Duox* genes was induced in the thyroid of *Duoxa*$^{-/-}$ mice.

DUOX protein level, like *Duox* mRNAs, was also elevated in the thyroids of *Duoxa*$^{-/-}$ mice. In the colon of *Duoxa*$^{-/-}$ mice, however, DUOX protein expression was greatly diminished despite intact mRNA expression, a finding consistent with reduced stability of the isolated DUOX subunits expressed without DUOXA heterodimerization partner in heterologous cell lines (21-23). Apart from cell type specific differences in protein stability, it is conceivable that in the thyroid of *Duoxa*$^{-/-}$ mice, lower DUOX protein stability may be surmounted by induction of DUOX mRNA expression.

DUOX proteins are normally expressed as high mannose glycosylated forms (180 kDa) in the endoplasmic reticulum (ER) and as fully glycosylated forms (~190 kDa) found at the plasma membrane (24, 25). That *Duoxa*$^{-/-}$ mice express DUOX exclusively in the immature, high mannose glycosylated form was confirmed by testing the sensitivity of the N-glycosylation to digestion with endoglycosidase H (Fig. 1G). The processing of endogenous DUOX in cells of *Duoxa*$^{-/-}$ mice is therefore reminiscent to that of recombinant DUOX expressed without DUOXA in heterologous systems *in vitro*. In the latter systems, the ER retained DUOX protein is completely inactive.

To more directly confirm the absence of DUOX-based NADPH oxidase activity, we determined H_2O_2 release from thyroid tissue of WT, *Duoxa*$^{+/-}$, and *Duoxa*$^{-/-}$ mice. We found that basal H_2O_2 release of thyroid tissue from *Duoxa*$^{-/-}$ mice, compared to that from WT or *Duoxa*$^{+/-}$ mice, was >5-fold lower. H_2O_2

release from the thyroid tissue samples of WT and Duoxa$^{+/-}$ mice, but not Duoxa$^{-/-}$ mice, was induced by ionomycin/PMA co-stimulation. Overall the stimulated H_2O_2 release from thyroid tissue was over 12 times higher in WT compared to Duoxa$^{-/-}$ mice (P=0.02). These results indicate loss of Ca^{2+}-inducible NADPH oxidase activity in the thyroids of Duoxa$^{-/-}$ mice. They also indicate that the amounts of H_2O_2 arising from cellular metabolism or other NADPH oxidases that permeate into the extracellular milieu are negligible compared to H_2O_2 generated by DUOX enzymes at the cell surface.

Cretinism of *Duoxa*$^{-/-}$ mice

Duoxa$^{-/-}$ mice appeared normal at birth and the genotype ratios were consistent with expected single-locus Mendelian inheritance (*Duoxa*$^{+/+}$:*Duoxa*$^{+/-}$:*Duoxa*$^{-/-}$=73:150:87; P=0.45, chi-square test). Complete loss of DUOX activity did therefore not cause embryonic lethality or affect prenatal growth. However, *Duoxa*$^{-/-}$ mice showed severely delayed postnatal development (Fig. 2A). Average age of eye opening, a marker for cerebral maturation, was delayed from 12.2 days in WT to 15.5 days in *Duoxa*$^{-/-}$ (P<0.0001) (Fig. 2F). Stunted growth became readily apparent at two weeks of age (body weight [g]: *Duoxa*$^{-/-}$ 5.8±0.1 *vs* WT 7.7±0.2; P<0.0001) (Fig. 2D). Whole mount bone stains revealed impaired linear growth of long bones, delayed enchondral ossification, and reduced bone mineralization in *Duoxa*$^{-/-}$ animals compared to WT littermates (Fig. 2E). *Duoxa*$^{-/-}$ mice did not survive weaning at P21. However, a substantial proportion of *Duoxa*$^{-/-}$ mice (>80%) survived into adult hood when weaned at P30. All *Duoxa*$^{-/-}$, but neither WT nor *Duoxa*$^{+/-}$ mice, displayed persistent abnormalities in motor function and coordination reflected by bilateral dystonic hind-limb clasping when lifted up by the tail and failure to invert and climb down when placed on a vertical pole. Between one and three months of age, approximately one third of *Duoxa*$^{-/-}$ mice developed signs of respiratory distress accompanied by an audible inspiratory stridor (Supplemental movie 1). Examination of the laryngotracheal units in these mice revealed subglottic stenoses due to extrinsic compression by massively enlarged thyroid glands.

Dwarfism and severe developmental delay are hallmarks of untreated CH (cretinism). Thyroid function tests using sensitive radioimmunoassays revealed undetectable level of T4 (<0.25 μg/dL), T3

(<50 ng/dL), and reverse-T3 (<2.5 ng/dL) in *Duoxa*$^{-/-}$ mice, whereas TSH concentrations were 500-fold (males) to 2500-fold (females) higher than in WT littermates (Fig. 2B, 2C). Heterozygous animals of every age tested (P6, P14, adult) had thyroid function parameters indistinguishable from age-matched WT animals. Thus, there was no apparent *Duoxa* haploinsufficiency with respect to thyroid function.

Histological examination of 2-months-old *Duoxa*$^{-/-}$ mice revealed diffuse, homogeneous hyperplasia of the thyroid gland with residual small follicles lined by columnar epithelium that frequently formed papillary folds protruding into the lumen (Fig. 3D, F). Immunochemical staining of TSH-ß in the anterior pituitary of *Duoxa*$^{-/-}$ mice showed massive hypertrophy and hyperplasia of the thyrotrophic cells (Fig. 3H). Overall, these findings indicate that the primary hypothyroidism of *Duoxa*$^{-/-}$ mice is due to dyshormonogenesis and consistent with a role of DUOX-derived H_2O_2 in driving thyroid peroxidase-catalyzed reactions.

Lack of thyroidal iodide organification in *Duoxa*$^{-/-}$ mice

To further characterize the hormone synthesis defect in *Duoxa*$^{-/-}$ mice, we investigated the thyroidal uptake and perchlorate-induced discharge of iodine-125 (^{125}I). To facilitate efficient uptake of the tracer in WT and heterozygous animals, all animals were fed a low-iodine diet (LID) for two weeks. TSH level of WT mice on LID were 40-fold higher compared to those on iodine-sufficient diet (Fig. 4A). LID failed to further increase the markedly elevated TSH level of *Duoxa*$^{-/-}$ mice suggesting maximal stimulation of the thyrotrophic cells in the absence of negative feedback by thyroid hormones. To study the kinetics of thyroidal ^{125}I uptake, the tracer was injected intraperitoneally and the accumulation of radioactivity over the anterior neck monitored with a gamma positioning system (Fig. 4B). The amount of activity detected over the midsternum was used as surrogate for change in background activity due to ^{125}I distribution in extrathyroidal tissues (Fig. 4C). While both WT and *Duoxa*$^{-/-}$ animals showed a rapid increase of ^{125}I activity over the thyroid position within the initial five minutes, only WT animals showed a further increase of activity over the ensuing four hours. Concurrently, non-thyroidal ^{125}I activity measured over the midsternum showed a steep decline from the initial peak (at 6 min) only in WT but not *Duoxa*$^{-/-}$ mice.

These results were consistent with a lack of clearance of ^{125}I from the circulation in *Duoxa*$^{-/-}$ mice due to limited accumulation in the thyroid gland. In fact, four hours after injection of ^{125}I over 60% of the initial dose was found in the excised thyroid gland of WT animals, whereas only about 14% of the dose had accumulated in the thyroid glands of *Duoxa*$^{-/-}$ mice (Fig. 4E).

To test whether the lower ^{125}I accumulation in the thyroid glands *Duoxa*$^{-/-}$ mice was due to loss of organification of iodide, the radioactivity over the neck was monitored after the injection of perchlorate (ClO_4^-). ClO_4^- is a competitive inhibitor of the sodium-iodide symporter at the basolateral membrane of follicular thyroid cells. Free iodide that has been concentrated in the gland but not been organified (bound to protein) should be subject to wash out after ClO_4^- administration and leak back into the circulation. Within one min of injection of ClO_4^-, a rapid loss of ^{125}I activity over the neck occurred in *Duoxa*$^{-/-}$ mice with over 50% loss of activity after 5 min (Fig. 4D). To corroborate these results, the accumulation of ^{125}I in thyroid glands dissected before and 20 min after ClO_4^- administration was determined by gamma counting. Glands of *Duoxa*$^{-/-}$ animals dissected before ClO_4^- injection contained 14.4±2.3% of the injected dose compared to only 6.6±0.9% after ClO_4^- indicating 54% washout (95% CI=22.7-84.8; P=0.0027) (Fig. 4E). The concomitant increase of ^{125}I activity in the blood was quantitatively consistent with the loss of activity in the thyroid glands (Fig. 4F). There was no significant ^{125}I washout from the thyroid glands of WT or heterozygous (*Duoxa*$^{+/-}$) mice.

The high ^{125}I activity in the circulation of *Duoxa*$^{-/-}$ mice together with the fact that their thyroid glands are massively enlarged and highly vascularized causes a high level of background activity in the perchlorate discharge test and, thus, relatively low fractional washout. To better assess the severity of the iodide organification defect, we directly tested the iodination status of TG protein. Analysis of thyroidal protein extracts by SDS-PAGE and autoradiography revealed that *Duoxa*$^{-/-}$ animals, in contrast to WT animals, did not incorporate ^{125}I into thyroglobulin (Fig. 4G). Note that the amount of thyroidal TG protein in WT animals on LID was not different from that of *Duoxa*$^{-/-}$ mice kept on either LID or normal diet, but substantially lower compared to WT animals on normal diet. These results are consistent with rapid turnover of TG in thyroid glands under excessive TSH stimulation. Consistently, the depletion of

TG in the thyroid glands of *Duoxa*$^{-/-}$ mice was ameliorated by supplementation of L-T4. In these animals fed an iodine-sufficient diet, TG protein of WT, but not that of *Duoxa*$^{-/-}$ mice, was clearly detectable on Western blots with antibodies specific for iodinated TG epitopes (Fig. 4H). L-T4 replacement increased total but not iodinated TG level in *Duoxa*$^{-/-}$ mice confirming that loss of iodide organification is not secondary to altered thyroidal TG metabolism.

Rescue of *Duoxa*$^{-/-}$ mice by L-T4 replacement

The Duox enzymes are not only expressed in thyroid epithelial cells, but also at high level in extrathyroidal organs particularly epithelial cells lining the GI-tract and the upper airways. To test whether the observed phenotype can be completely attributed to the lack of thyroid hormone production, *Duoxa*$^{-/-}$ animals were maintained on a hormone replacement regimen starting from P6 with daily subcutaneous or intraperitoneal injections of L-T4. *Duoxa*$^{-/-}$ mice on chronic L-T4 replacement had normalized circulating levels of the active thyroid hormone T3 (*Duoxa*$^{-/-}$ 90.0±4.2 [n=8] vs WT 87.4±6.1 [n=7]). Their bone growth, weight gain (Fig. 2D) and fertility were indistinguishable from that of WT littermates and they did not display any of the signs or symptoms described in untreated *Duoxa*$^{-/-}$ mice. Differences in relative organ weights between *Duoxa*$^{-/-}$ and WT animals were also obliterated by L-T4 replacement (Fig. 2G). In addition, on a survey including thyroid glands, airways and the entire gastrointestinal tract no histomorphological differences were observed between WT and L-T4 substituted *Duoxa*$^{-/-}$ mice.

DISCUSSION

In this study we showed that mice deficient in both *Duoxa1* and *Duoxa2* lack detectable thyroid hormone production due to a total iodine organification defect. In heterologous systems *in vitro*, expression of recombinant DUOX without co-expression of DUOXA does not reconstitute a functional, surface-expressed NADPH oxidase. Here we showed that in mice with inactivation of both *Duoxa* genes, endogenous DUOX similarly remains in an immature, ER-retained form and lacks Ca^{2+}/PKC-inducible H_2O_2 release. Thus *Duoxa*$^{-/-}$ mice provide a model for complete deficiency of DUOX-based NADPH oxidases. Having undetectable thyroid hormone production and ^{125}I incorporation into thyroglobulin these mice provide irrefutable evidence that only DUOX-generated H_2O_2, but not ROS from other sources, is able to drive thyroid hormone synthesis.

Although both DUOX isoenzymes are expressed in follicular thyroid cells, only the thyroid function of DUOX2 has been unambiguously established. In humans, loss of function mutations in *DUOX2* and *DUOXA2* underlie iodide organification defects in a subset of patients with CH (reviewed in (26)). Apart from a large deletion affecting both DUOX systems, no mutations in *DUOX1/DUOXA1* have been found in CH patients. The *in vivo* function of the DUOX1 system remains unclear. It is expressed in many of the same tissues as DUOX2, though frequently at lower level (e.g. in thyroid, GI-tract). Like DUOX2, it is a Ca^{2+}-stimulated H_2O_2 generating NADPH oxidase, but there are clearly differences in regulation of gene expression (27) and intrinsic enzyme activity (3).

Two mouse models with deficiency in either the *Duox1* or *Duox2* system have been described. A model for *Duox2* deficiency was provided by the discovery of the *thyd* strain harboring a spontaneous missense mutation (V674G) at a conserved position of *Duox2* (12). While *Duox2*^{thyd} mice showed retarded growth similar to *Duoxa*$^{-/-}$ mice, there is no reported detrimental effect on survival during the weaning or postweaning period. It is likely that residual iodide organification in *Duox2*^{thyd} mice accounts for this difference. Apart from the possibility that the *thyd* mutation is hypomorphic, mitigation of the defect could be provided by the intact *Duox1* system as has been proposed for CH patients with complete loss of *DUOX2*. Indeed, in male *Duox2*^{thyd} mice, average serum T4 level is 0.5 µg/dl (12), whereas T4

level of *Duoxa*$^{-/-}$ was below the detection limit (<0.25 µg/dl). Similarly, serum TSH level measured in our radioimmunoassay (12, 28) were 200-fold and 500-fold over baseline in male *Duox2*^{thyd} and *Duoxa*$^{-/-}$ mice, respectively. Since serum TSH was not further augmented in *Duoxa*$^{-/-}$ mice placed on LID, maximal disinhibition of thyrotrophs from negative feedback had been reached on a normal, iodine-sufficient diet. This finding in turn indicates that T4 is not only undetectable but essentially excludes the presence of physiologically relevant amounts of T4 in *Duoxa*$^{-/-}$ mice.

In contrast to *Duox2*^{thyd} mice, *Duox1* deficient mice did not display an obvious phenotype and have normal thyroid function profiles (13). Clearly, a redundant role of *Duox1* in thyroid hormone synthesis would not satisfactorily explain the evolutionary pressure that maintained a duplicated *Duox*/*Duoxa* locus since the teleost-amphibian divergence. One plausible explanation for the presence of two functional DUOX systems could have been redundancy for a particularly vital role of DUOX-generated H_2O_2 in development. For instance, in invertebrates having only one functional copy of each *Duox* and *Duoxa* genes, the loss of function mutations in either leads to severe developmental abnormalities with high mortality at an early developmental stage ((14, 15, 18, 19)). Reduced survival of these mutants has been attributed to an important function of DUOX in driving di-tyrosine cross linking reactions of extracellular matrix proteins during larval development, peroxidative reactions analogous to the cross linking of iodotyrosines to iodothyronines (14). However, our results convincingly exclude redundancy of DUOX isoenzymes for an essential role during prenatal murine development since *Duoxa*$^{-/-}$ mice were born at expected Mendelian ratios and did not show postnatal abnormalities, other than those that could be prevented by early hormone replacement.

It is therefore more likely that the presence of two DUOX paralogs relates to their differential regulation in extra-thyroidal organs. A common theme of DUOX function in various model systems is their adaptive response to environmental stressors. In invertebrates, *Duox* is strongly upregulated in the intestinal epithelium upon pathogen exposure and RNAi-mediated knockdown of *Duox* (15, 18) or Duoxa (18) diminishes ROS production and severely impairs the ability to clear pathogens. In acute epithelial injury in zebrafish, H_2O_2 produced locally by activated DUOX acts as chemoattractant signal to recruit

leukocytes (29). There is also ample evidence for strong induction of DUOX in mammalian species as part of innate immune responses, e.g. in bacterial (30) or nematode (31) infections in the intestine, chronic inflammatory bowel diseases (32, 33), or airway inflammation (34).

Duoxa$^{-/-}$ mice on L-T4 replacement should be a useful mammalian model system to screen for extrathyroidal functions of DUOX in response to environmental challenges. The DUOX isoenzymes are often co-expressed in the same tissues raising the possibility of at least partial functional redundancy. Since the proximity of the DUOX genes precludes intergenic meiotic recombinations, double gene knockouts cannot be readily obtained by crossing lines of mice with single gene defects (such as, *Duox2*^{thyd} and *Duox1*$^{-/-}$ mice). In this regard, *Duoxa*$^{-/-}$ mice provide a unique model of complete deficiency of functional DUOX-based NADPH oxidases.

MATERIALS AND METHODS

Animals

All procedures carried out in mice and described below were approved by the animal ethics committees at the University of Chicago, the University of Michigan, and Free University of Brussels, respectively. Animals were maintained in specific pathogen-free conditions on a 12-hour light/12-hour dark cycle (light on at 06:00) and fed an autoclaved laboratory chow and tap water *ad libitum*. The mice on L-thyroxine (L-T4; L-thyroxine sodium salt pentahydrate; Sigma) replacement received 40 ng L-T4/g body weight by daily subcutaneously injection starting from P6. After weaning, thyroid hormone replacement was achieved by providing albuminized drinking water containing 0.26 mg/l L-T4.

Generation of targeting construct

The targeting construct for generation of *Duoxa*$^{-/-}$ mice was designed to delete a 2,857 bp region extending from exon 5 of *Duoxa2* to coding exon 5 of *Duoxa1*. Termination of translation at the breakpoints was ensured by the additional insertion of stop codons in the reading frames of the *Duoxa* genes (after codon 246 in *Duoxa1*; after codon 232 of *Duoxa2*). The DTA cassette was excised (via *Kpn*I and *Nhe*I) from the pPGKneoDTA vector (kindly provided by Philippe Soriano) and the ACN cassette (via *EcoR*I and *Kpn*I) from plasmid pACN (kindly provided by Mario Capecchi) and three-fragments ligation performed with the *Nhe*I/*EcoR*I digested pMCS5 plasmid (MoBiTec). The ACN cassette was flanked with loxP sites and contains the neomycin resistance (Neo^{R}) gene under control of the mouse RNA Pol II promoter, together with Cre recombinase under the control of the testis-specific promoter of angiotensin-converting enzyme (tACE-CRE). The DTA (diphtheria toxin subunit A) cassette was used for negative selection against non-homologous recombination. The homology arms were then amplified from isogenic genomic DNA from the 126/S6 ES cell line using high-fidelity Pfu polymerase (Stratagene). The 4.7 kb long arm fragment was cloned via *Pme*I/*BsiW*I sites. Subsequently, the 2.1 kb short arm fragment was prepared with terminal *BamH*I sites and ligated into the *Bgl*II site to obtain the targeting vector. A

clone of the final construct was confirmed by restriction digestion and bidirectional sequencing, linearized with *Pme*I and purified by gel extraction.

Generation of targeted embryonic stem (ES) cells and mutant mice

The linearized targeting construct was electroporated into feeder-less 129S6 ES cells. After selection with G418 (200 μg/ml), 9 out of 144 (6.25%) neomycin-resistant ES cell clones were found to be correctly targeted as shown by long-range PCR assays and Southern blotting (Supplemental Fig. S1). Positive ES cell clones were injected into C57BL/6J blastocysts at the University of Chicago Transgenic Core Facility. Germline transmitting chimeras were mated with C57BL/6J WT females. In ES-cell derived germ cells of chimeric mice, CRE expression leads to excision of the ACN cassette during spermatogenesis, with only a single loxP element (flanked by the stop codons inserted in the *Duoxa* ORFs) remaining. Heterozygous F1 transgenic mice were identified by coat color (agouti) and by PCR of DNA isolated from tail tips. All data reported here were obtained from F2 hybrid (F1 intercross) animals originating from a single ES cell clone (clone 43). The basic characteristics of the phenotype (growth retardation, thyroid function tests) were confirmed in *Duoxa*$^{-/-}$ mice derived from two additional independently targeted ES cell clones (clones 40 and 60) and in *Duoxa*$^{-/-}$ mice maintained either on a pure 129S6/SvEvTac background or backcrossed for over six generations with C57BL/6J mice.

Genotyping

Crude genomic DNA extracts from toe clips (P9-12) and PCR amplification were performed using the REDExtract-N-Amp Tissue PCR Kit (Sigma). PCR was performed with three primers, including the common primer DA-WT/KO-F:5'-CAGCAGTCCTGGTCAGGGA-3', a WT allele-specific primer DA-WT-R: 5'-CCTGCTACGGAGACGAACA-3', and a KO allele-specific primer DA-KO-R: 5'-ACATCTTCTGCCTAGGTCCTG-3'. PCR products were separated on 1.5% agarose gels. Presence of the WT allele is evident by a 381 bp fragment, whereas the amplicon from the KO allele has a size of 568 bp.

Thyroid function tests

Serum total tetraiodothyronine (thyroxine; T4), triiodothyronine (T3), and reverse triiodothyronine (rT3) concentrations were measured by coated tube RIAs (Diagnostic Products). Serum thyroid-stimulating hormone (thyrotropin; TSH) was determined using a sensitive, heterologous, disequilibrium, double-antibody precipitation RIA (28).

Immunohistochemistry

4-µm-thick sections from paraffin-embedded specimens were deparaffinized, rehydrated, and subjected to antigen retrieval in 10 mM citrate buffer, pH 6.0 for 20 min at 95C. Sections were then washed with PBS and incubated with either mouse monoclonal antibodies against TG (clone 14/14; Cell Sciences, Canton, MA) or rabbit anti-rat TSH beta-IC-1 (AFP1274789, NIDDK). Specific antigen-antibody complexes were revealed using horseradish peroxidase (HRP)-conjugated secondary antibodies (ImmPRESS universal antibody; Vector Laboratories, Burlingame, CA) and the chromogen substrate NovaRED (Vector Laboratories). Sections were counterstained with Mayer's hematoxylin, dehydrated and permanently mounted in non-aqueous medium (VectaMount; Vector Laboratories).

Whole-mount skeletal preparations

To assess endochondral ossification at early postnatal stages of development, bone and cartilage were simultaneously visualized by whole-mount staining with Alizarin Red and Alcian Blue, respectively. Briefly, after removal of skin and evisceration, carcasses were fixed for three days in 95% ethanol. Following fat removal by incubation in acetone the specimens were stained for three days with Alcian Blue 8GX (15 mg/ml) and Alizarin Red (5 mg/ml) in 5% glacial acetic acid/60% ethanol. Samples were cleared over several weeks in 1% KOH with increasing concentrations (0-80%) of glycerol before storage in 100% glycerol. Photographs were taken using bright-field optics and transillumination with the specimens submerged in glycerol.

SDS-PAGE and Western blotting

For detection of DUOX proteins, mouse tissues were extracted in lysis buffer (50mM phosphate buffer, 20mM EDTA, 1% triton X-100) supplemented with a mixture of protease inhibitors (Complete; Roche Applied Science) for 1h at 4°C. The lysate was centrifuged 15 min at 10,000 rpm, and solubilized proteins were denatured in Laemmli buffer (pH 6.8; 1.54% DTT, 2% SDS, 10% glycerol and 0.75% Tris) before loading and separation by SDS-PAGE electrophoresis. DUOX proteins were detected with anti-DUOX antibody (1/1000; (2)). Probing with anti-protein disulfide isomerase (PDI) antibodies (Santa Cruz Biotech.) was used as loading control. Fluorescent secondary antibodies (1/10,000; IRDye800 anti-rabbit and IRDye680 anti-mouse; LI-COR, Lincoln, NE) were used for image acquisition and quantification with the Odyssey infrared imaging system (LI-COR).

For the deglycosylation experiments, proteins were extracted on ice for 30 min in a 50 mM citrate buffer, pH 5.5, 20 mM EDTA, 1% Triton X-100 supplemented with protease inhibitors. Soluble proteins were treated for 30 min at 30°C with 10 mU of endoglycosidase H (Roche). As negative control, the same soluble fraction was treated without enzyme under the same conditions. Treated proteins were denatured in Laemmli buffer, separated by SDS-PAGE, and detected with the anti-DUOX antibody as described above.

For the detection of TG in mouse thyroids by Western blotting, total protein extracts (3 µg/lane) were separated by 6% SDS-PAGE and transferred to PVDF membrane (Millipore). Total thyroglobulin proteins were immunodetected with anti-bovine TG rabbit serum (1:12,000; (35)); the iodinated thyroglobulin forms were specifically revealed with a monoclonal antibody (B2, 1:5,000; (36)).

To detect thyroidal ^{125}I organification, glands were homogenized in lysis buffer (50 mM Tris-HCl (pH 8.0), 150 mM NaCl, 1 mM DTT, 1% Nonidet P-40 supplemented with protease inhibitors) and cleared by centrifugation (12,000 g, 15 min, 4 C). Soluble protein extracts (50 µg/lane) were separated on 4% SDS-PAGE under reducing and non-reducing conditions. Gels were fixed in methanol/acetic acid and stained with colloidal Coomassie Blue (37). Vacuum dried gels were exposed to autoradiography films.

Assay for H_2O_2 release from thyroid tissue

The thyroid glands were dissected, cut in small pieces and rinsed extensively in Krebs–Ringer Hepes medium (KRH; (38)). About two thyroid lobes were used for each experimental condition. The tissues were incubated with or without 2µM ionomycin (Sigma) + 5µM phorbol 12-myristate 13-acetate (PMA; Sigma) during 3h at 37°C in the KRH medium supplemented with 0.1mg/ml horseradish peroxidase type II (Sigma) and 440mM homovanillic acid (Sigma). The fluorescence intensity from the KRH medium was measured on a microplate reader (TECAN Infinite F200 PRO) with excitation at 315 nm and emission at 415 nm. H_2O_2 concentrations were estimated based on standard curves obtained with known concentrations of H_2O_2 run in the same experiment. All measurements were corrected for auto-fluorescence of the medium. The H_2O_2 production was normalized to the total DNA content of the incubated tissue and expressed in µM of H_2O_2 per µg of DNA.

Reverse transcription of mRNA and realtime semiquantitative PCR

Total RNA was prepared using TRIzol reagent (Invitrogen). After DNase digestion, RNA was further cleaned up with the RNeasy Mini Kit (QIAGEN). RNA (0.5 µg) was reverse transcribed with Superscript II (Invitrogen). PCR amplifications were performed using a C1000 Thermal Cycler (Bio-Rad) with SYBR Green dye (Molecular Probes, Carlsbad, CA) and Platinum Taq DNA polymerase (Invitrogen). Each reaction was performed in triplicates with the following conditions: 3 min at 95°C, 40 cycles of 9 s at 95°C, and 1 min at 60°C, followed by 1 min at 55°C. Melting curve analysis was used to confirm amplification specificity. Gene expression was normalized to *Polr2a* mRNA. The sequences of primers are listed in Supplemental Table S1.

^{125}I uptake and perchlorate discharge test

^{125}I (8 µCi/mouse; approximately $1.7x10^7$ cpm) was given i.p. after feeding mice with low iodine diet (<0.05 ppm iodine; Harlan Teklad Co.) for two weeks. Serum samples for thyroid function tests were

obtained 24 hours before the uptake experiments. *In vivo* kinetics of thyroidal ^{125}I accumulation was recorded by counting over the neck using a gamma positioning system (Navigator GPS, RMD Instruments Corp). To obtain the average uptake rate at 4 hours, animals were sacrificed and their thyroid glands dissected immediately. The amount of radioactivity in blood samples and excised thyroid glands was measured in a γ counter (Cobra II Auto-Gamma, Packard) and expressed as fraction of the injected dose. For the perchlorate-induced iodide discharge test, 10 μg/g body weight $KClO_4$ was injected i.p. 4 hours after ^{125}I administration, and thyroid glands obtained 20 min later. To monitor changes of ^{125}I activity in the circulation, blood samples were obtained from the retro-orbital plexus with a heparinated micropipette before and 20 min after perchlorate administration. For calculation of the fraction of ^{125}I dose in the circulation, total blood volume (in ml) was estimated as 7.2% of the body weight (in g) (39).

Statistics

Unless indicated otherwise, statistical analysis was performed using unpaired, two-tailed Student's *t* test (Prism 5, GraphPad software) and data presented as means±SEM. Differences were considered significant at $P<0.05$.

ACKNOWLEDGMENTS

We are grateful to Linda Degenstein and Xiu Chen (Transgenic Core Facility, U of Chicago) for their expert technical assistance.

REFERENCES

1. **Dupuy C, Ohayon R, Valent A, Noel-Hudson MS, Deme D, Virion A** 1999 Purification of a novel flavoprotein involved in the thyroid nadph oxidase. Cloning of the porcine and human cdnas. J Biol Chem 274:37265-9
2. **De Deken X, Wang D, Many MC, Costagliola S, Libert F, Vassart G, Dumont JE, Miot F** 2000 Cloning of two human thyroid cdnas encoding new members of the nadph oxidase family. J Biol Chem 275:23227-33
3. **Rigutto S, Hoste C, Grasberger H, Milenkovic M, Communi D, Dumont JE, Corvilain B, Miot F, De Deken X** 2009 Activation of dual oxidases duox1 and duox2: Differential regulation mediated by camp-dependent protein kinase and protein kinase c-dependent phosphorylation. J Biol Chem 284:6725-34
4. **Corvilain B, van Sande J, Laurent E, Dumont JE** 1991 The H_2O_2-generating system modulates protein iodination and the activity of the pentose phosphate pathway in dog thyroid. Endocrinology 128:779-85
5. **Bjorkman U, Ekholm R** 1988 Accelerated exocytosis and H_2O_2 generation in isolated thyroid follicles enhance protein iodination. Endocrinology 122:488-94
6. **Grasberger H, Refetoff S** 2006 Identification of the maturation factor for dual oxidase. Evolution of an eukaryotic operon equivalent. J Biol Chem 281:18269-72
7. **Fischer H, Gonzales LK, Kolla V, Schwarzer C, Miot F, Illek B, Ballard PL** 2007 Developmental regulation of duox1 expression and function in human fetal lung epithelial cells. Am J Physiol Lung Cell Mol Physiol
8. **Luxen S, Belinsky SA, Knaus UG** 2008 Silencing of duox nadph oxidases by promoter hypermethylation in lung cancer. Cancer Res 68:1037-45
9. **Zamproni I, Grasberger H, Cortinovis F, Vigone MC, Chiumello G, Mora S, Onigata K, Fugazzola L, Refetoff S, Persani L, Weber G** 2008 Biallelic inactivation of the dual oxidase maturation factor 2 (duoxa2) gene as a novel cause of congenital hypothyroidism. J Clin Endocrinol Metab 93:605-10
10. **Morand S, Ueyama T, Tsujibe S, Saito N, Korzeniowska A, Leto TL** 2009 Duox maturation factors form cell surface complexes with duox affecting the specificity of reactive oxygen species generation. Faseb J 23:1205-18
11. **Grasberger H** 2010 Defects of thyroidal hydrogen peroxide generation in congenital hypothyroidism. Mol Cell Endocrinol 322:99-106
12. **Johnson KR, Marden CC, Ward-Bailey P, Gagnon LH, Bronson RT, Donahue LR** 2007 Congenital hypothyroidism, dwarfism, and hearing impairment caused by a missense mutation in the mouse dual oxidase 2 gene, duox2. Mol Endocrinol 21:1593-602
13. **Donko A, Ruisanchez E, Orient A, Enyedi B, Kapui R, Peterfi Z, De Deken X, Benyo Z, Geiszt M** 2010 Urothelial cells produce hydrogen peroxide through the activation of duox1. Free Radic Biol Med 49:2040-8
14. **Edens WA, Sharling L, Cheng G, Shapira R, Kinkade JM, Lee T, Edens HA, Tang X, Sullards C, Flaherty DB, Benian GM, Lambeth JD** 2001 Tyrosine cross-linking of extracellular matrix is catalyzed by duox, a multidomain oxidase/peroxidase with homology to the phagocyte oxidase subunit gp91phox. J Cell Biol 154:879-91
15. **Ha EM, Oh CT, Bae YS, Lee WJ** 2005 A direct role for dual oxidase in drosophila gut immunity. Science 310:847-50
16. **El Hassani RA, Benfares N, Caillou B, Talbot M, Sabourin JC, Belotte V, Morand S, Gnidehou S, Agnandji D, Ohayon R, Kaniewski J, Noel-Hudson MS, Bidart JM, Schlumberger M, Virion A, Dupuy C** 2005 Dual oxidase2 is expressed all along the digestive tract. Am J Physiol Gastrointest Liver Physiol 288:G933-42
17. **Geiszt M, Witta J, Baffi J, Lekstrom K, Leto TL** 2003 Dual oxidases represent novel hydrogen peroxide sources supporting mucosal surface host defense. Faseb J 17:1502-4

18. **Chavez V, Mohri-Shiomi A, Garsin DA** 2009 Ce-duox1/bli-3 generates reactive oxygen species as a protective innate immune mechanism in caenorhabditis elegans. Infect Immun 77:4983-9
19. **Xie X, Hu J, Liu X, Qin H, Percival-Smith A, Rao Y, Li SS** 2010 Nip/duoxa is essential for drosophila embryonic development and regulates oxidative stress response. Int J Biol Sci 6:252-67
20. **Bunting M, Bernstein KE, Greer JM, Capecchi MR, Thomas KR** 1999 Targeting genes for self-excision in the germ line. Genes Dev 13:1524-8
21. **Grasberger H, X DED, Miot F, Pohlenz J, Refetoff S** 2007 Missense mutations of dual oxidase 2 (duox2) implicated in congenital hypothyroidism have impaired trafficking in cells reconstituted with duox2 maturation factor. Mol Endocrinol
22. **Luxen S, Noack D, Frausto M, Davanture S, Torbett BE, Knaus UG** 2009 Heterodimerization controls localization of duox-duoxa nadph oxidases in airway cells. J Cell Sci 122:1238-47
23. **Hoste C, Rigutto S, Van Vliet G, Miot F, De Deken X** 2010 Compound heterozygosity for a novel hemizygous missense mutation and a partial deletion affecting the catalytic core of the h2o2-generating enzyme duox2 associated with transient congenital hypothyroidism. Hum Mutat 31:E1304-19
24. **De Deken X, Wang D, Dumont JE, Miot F** 2002 Characterization of thox proteins as components of the thyroid h(2)o(2)-generating system. Exp Cell Res 273:187-96
25. **Morand S, Chaaraoui M, Kaniewski J, Deme D, Ohayon R, Noel-Hudson MS, Virion A, Dupuy C** 2003 Effect of iodide on nicotinamide adenine dinucleotide phosphate oxidase activity and duox2 protein expression in isolated porcine thyroid follicles. Endocrinology 144:1241-8
26. **Grasberger H, Refetoff S** 2011 Genetic causes of congenital hypothyroidism due to dyshormonogenesis. Curr Opin Pediatr 23:421-8
27. **Harper RW, Xu C, Eiserich JP, Chen Y, Kao CY, Thai P, Setiadi H, Wu R** 2005 Differential regulation of dual nadph oxidases/peroxidases, duox1 and duox2, by th1 and th2 cytokines in respiratory tract epithelium. FEBS Lett 579:4911-7
28. **Pohlenz J, Maqueem A, Cua K, Weiss RE, Van Sande J, Refetoff S** 1999 Improved radioimmunoassay for measurement of mouse thyrotropin in serum: Strain differences in thyrotropin concentration and thyrotroph sensitivity to thyroid hormone. Thyroid 9:1265-71
29. **Niethammer P, Grabher C, Look AT, Mitchison TJ** 2009 A tissue-scale gradient of hydrogen peroxide mediates rapid wound detection in zebrafish. Nature 459:996-9
30. **Liu X, Lu R, Xia Y, Sun J** 2010 Global analysis of the eukaryotic pathways and networks regulated by salmonella typhimurium in mouse intestinal infection in vivo. BMC Genomics 11:722
31. **Athanasiadou S, Jones LA, Burgess ST, Kyriazakis I, Pemberton AD, Houdijk JG, Huntley JF** 2011 Genome-wide transcriptomic analysis of intestinal tissue to assess the impact of nutrition and a secondary nematode challenge in lactating rats. PLoS One 6:e20771
32. **Csillag C, Nielsen OH, Vainer B, Olsen J, Dieckgraefe BK, Hendel J, Vind I, Dupuy C, Nielsen FC, Borup R** 2007 Expression of the genes dual oxidase 2, lipocalin 2 and regenerating islet-derived 1 alpha in crohn's disease. Scand J Gastroenterol 42:454-63
33. **Hamm CM, Reimers MA, McCullough CK, Gorbe EB, Lu J, Gu CC, Li E, Dieckgraefe BK, Gong Q, Stappenbeck TS, Stone CD, Dietz DW, Hunt SR** 2010 Nod2 status and human ileal gene expression. Inflamm Bowel Dis 16:1649-57
34. **Moskwa P, Lorentzen D, Excoffon KJ, Zabner J, McCray PB, Jr., Nauseef WM, Dupuy C, Banfi B** 2007 A novel host defense system of airways is defective in cystic fibrosis. Am J Respir Crit Care Med 175:174-83
35. **Roger PP, Van Heuverswyn B, Lambert C, Reuse S, Vassart G, Dumont JE** 1985 Antagonistic effects of thyrotropin and epidermal growth factor on thyroglobulin mrna level in cultured thyroid cells. Eur J Biochem 152:239-45
36. **Den Hartog MT, De Boer M, Veenboer GJ, De Vijlder JJ** 1990 Generation and

characterization of monoclonal antibodies directed against noniodinated and iodinated thyroglobulin, among which are antibodies against hormonogenic sites. Endocrinology 127:3160-5

37. **Encarnacion S, Hernandez M, Martinez-Batallar G, Contreras S, Vargas Mdel C, Mora J** 2005 Comparative proteomics using 2-d gel electrophoresis and mass spectrometry as tools to dissect stimulons and regulons in bacteria with sequenced or partially sequenced genomes. Biol Proced Online 7:117-35

38. **Milenkovic M, De Deken X, Jin L, De Felice M, Di Lauro R, Dumont JE, Corvilain B, Miot F** 2007 Duox expression and related h2o2 measurement in mouse thyroid: Onset in embryonic development and regulation by tsh in adult. J Endocrinol 192:615-26

39. **Diehl KH, Hull R, Morton D, Pfister R, Rabemampianina Y, Smith D, Vidal JM, van de Vorstenbosch C** 2001 A good practice guide to the administration of substances and removal of blood, including routes and volumes. J Appl Toxicol 21:15-23

40. **Gentile F, Palumbo G, Salvatore G** 1992 The origin of the electrophoretic doublet of thyroglobulin. Biochem Biophys Res Commun 186:1185-91

41. **Marino M, Zheng G, Chiovato L, Pinchera A, Brown D, Andrews D, McCluskey RT** 2000 Role of megalin (gp330) in transcytosis of thyroglobulin by thyroid cells. A novel function in the control of thyroid hormone release. J Biol Chem 275:7125-37

590 **FIGURE LEGENDS**

591

592 **FIG. 1.** Generation of *Duoxa*$^{-/-}$ mice. A) Structure of the *Duoxa1* and *Duoxa2* genes, the targeting
593 construct, and the final knockout allele. A unique *Pme*I endonuclease site was used to linearize the vector
594 before electroporation. Homologous recombination of ES cell DNA with the targeting construct replaced
595 a ~2.9 kbp region with the floxed ACN cassette modified by the addition of terminal stop codons in frame
596 of the *Duoxa* genes. The ACN cassette contained the *Neo*^{R} positive selection marker and encodes *Cre*
597 recombinase expressed specifically during spermatogenesis from a testis specific promoter (*tACE*).
598 Passage of the targeted locus through the germ line of male chimeras resulted in the self-excision of the
599 ACN cassette with only a single loxP site flanked by stop codons remaining. B) Strategy of genotyping.
600 The location of the three primers and the amplicons from WT and knockout alleles are indicated. C-D)
601 Expression of *Duox* and *Duoxa* mRNA in WT (n=6) and *Duoxa*$^{-/-}$ (n=5) thyroid glands (C) and
602 descending colon (D). E) DUOX protein expression in thyroid (40 µg total protein) and descending colon
603 (70 µg) of 3-month old WT and *Duoxa*$^{-/-}$ mice. Protein disulfide isomerase (PDI) was immunodetected to
604 validate equal protein loading. F) Determination of H_2O_2 release from thyroid tissue samples of mice
605 (pure 129S6/SvEvTac genetic background) with the indicated *Duoxa* genotypes. H_2O_2 concentrations
606 accumulating in the medium were normalized for DNA content of the tissue samples. G) Maturation of
607 DUOX N-glycosylation in WT and *Duoxa*$^{-/-}$ mice. Cecal protein extracts were analyzed on Western blots
608 with or without prior digestion with Endoglycosidase H (EndoH). Maturation of DUOX N-glycosylation
609 in the Golgi apparatus produces endoglycosidase H (Endo H) resistant glycans (*R*). DUOX protein from
610 *Duoxa*$^{-/-}$ mice is only detectable as EndoH sensitive glycoform (*S*) indicating complete retention of
611 DUOX in the endoplasmic reticulum (*ER*).

612

613 **FIG. 2.** Cretinism phenotype of *Duoxa*$^{-/-}$ mice. A) Exemplar 4-weeks-old *Duoxa*$^{-/-}$ and WT littermates. B,
614 C) Serum T4 and TSH concentrations in WT, heterozygous, and *Duoxa*$^{-/-}$ animals. *Blue* and *pink* filled
615 symbols denote males and females, respectively. D) Body weight of WT (in *black*), heterozygous (*grey*),

Duoxa$^{-/-}$ mice (*red*), and *Duoxa*$^{-/-}$ mice receiving L-T4 replacement starting from P6 (*yellow*). Note that *Duoxa*$^{-/-}$ without thyroid hormone replacement did not survive weaning at P21 and were, therefore, weaned at P30. E) Skeletal preparations (rib cage, knee joint, forelimb) from WT and *Duoxa*$^{-/-}$ mice at P13 stained with Alizarin Red (Bone) and Alcian Blue 8GX (Cartilage). F) Delayed eye opening of *Duoxa*$^{-/-}$ pups. The curves depict the fraction of mice with bilateral open eyes at the indicated postnatal age. Color coding is identical to panel D. WT: n=25; *Duoxa*$^{-/-}$: n=22; *Duoxa*$^{-/-}$/L-T4: n=13. G) Weights of selected organs in 2-months old mice normalized for total body weight. Untreated *Duoxa*$^{-/-}$ (*red* bars) displayed thyroid hyperplasia and hyposplenia. In contrast, liver weight was reduced proportionally to total body weight. Note that the absolute brain weights (i.e., not normalized for body weight) were not significant different between the genotypes. Organ weights of *Duoxa*$^{-/-}$ mice on L-T4 replacement are represented by *yellow* bars.

FIG. 3. Pathology of thyroid glands and anterior pituitary. A, B) Exemplar H&E-stained thyrotracheal units of a 2-months old *Duoxa*$^{-/-}$ mouse with manifest inspiratory stridor and a WT littermate. C, D) Immunohistochemical detection of TG on thyroid sections from mice in panel A. E, F) Exemplar micrographs of thyroid tissue from 10-months old mice. G, H) Detection of thyrotrophic cells in the anterior pituitary by immunochemical staining of TSH-ß subunit. I) Expression of selected thyroidal differentiation markers determined by real-time RT-PCR.

FIG. 4. Thyroidal ^{125}I organification. A) Effect of two weeks of low iodine diet (LID) on serum TSH concentrations of WT and *Duoxa*$^{-/-}$ mice. B-C) Kinetics of ^{125}I distribution in WT and *Duoxa*$^{-/-}$ mice. ^{125}I activity over the anterior neck (B) and the midsternum (C) was determined using a γ-positioning system. The plots shown are representative curves from individual animals. D) Perchlorate-induced change in ^{125}I activity recorded over the anterior neck. Four hours following administration of ^{125}I, perchlorate was given intraperitoneally and activity over the neck monitored for 20 minutes. Representative data from two mice are plotted for each genotype. E) Thyroidal ^{125}I activity before (*open bars*) and 20 min after (*black*

642 *filled bars*) administration of ClO_4^-. Activity of dissected thyrotracheal units was determined using a γ-
643 counter. Data are expressed in % of the administered dose (8 μCi/animal). Significant perchlorate-induced
644 loss of thyroidal ^{125}I activity was only observed in *Duoxa*$^{-/-}$ mice (53.7% washout [95% CI=22.7-84.8];
645 *P*=0.0027), but not WT (+/+) or heterozygous (+/-) animals. F) Perchlorate-induced appearance of ^{125}I
646 activity in the circulation. Four hours following injection of ^{125}I, blood was collected retro-orbitally before
647 and 20-min after administration of $KClO_4$. Bars represent the perchlorate-induced increase of ^{125}I activity
648 in blood, expressed as a percentage of the injected dose. Total blood volume (in ml) was estimated to be
649 7.2% of body weight (in g)(39). **, *P*<0.01; ***, *P*<0.001. G) Reducing SDS-PAGE of thyroidal protein
650 extracts (50 μg/lane) from mice on LID. Thyroids were collected at the end of the perchlorate discharge
651 tests. Protein was stained with colloidal Coomassie Brilliant Blue and ^{125}I incorporation revealed by
652 autoradiography. *S* and *F* denote *slow* and *fast* migrating forms of TG, respectively (40, 41). Extracts
653 analyzed are from two different WT and *Duoxa*$^{-/-}$ mice, respectively. H) Reducing SDS PAGE of
654 thyroidal protein extracts from mice on an iodine sufficient diet. Upper panel shows a Coomassie Blue
655 stained gel. Lower panel depicts a Western blot probed simultaneously with pan-TG antiserum (*green*
656 *signal*) and an antibody specific for iodinated TG (*red signal*) (36). In the color merge, iodinated and non-
657 iodinated forms of TG appear in yellow and green, respectively. Each lane corresponds to protein extract
658 from a different animal.
659

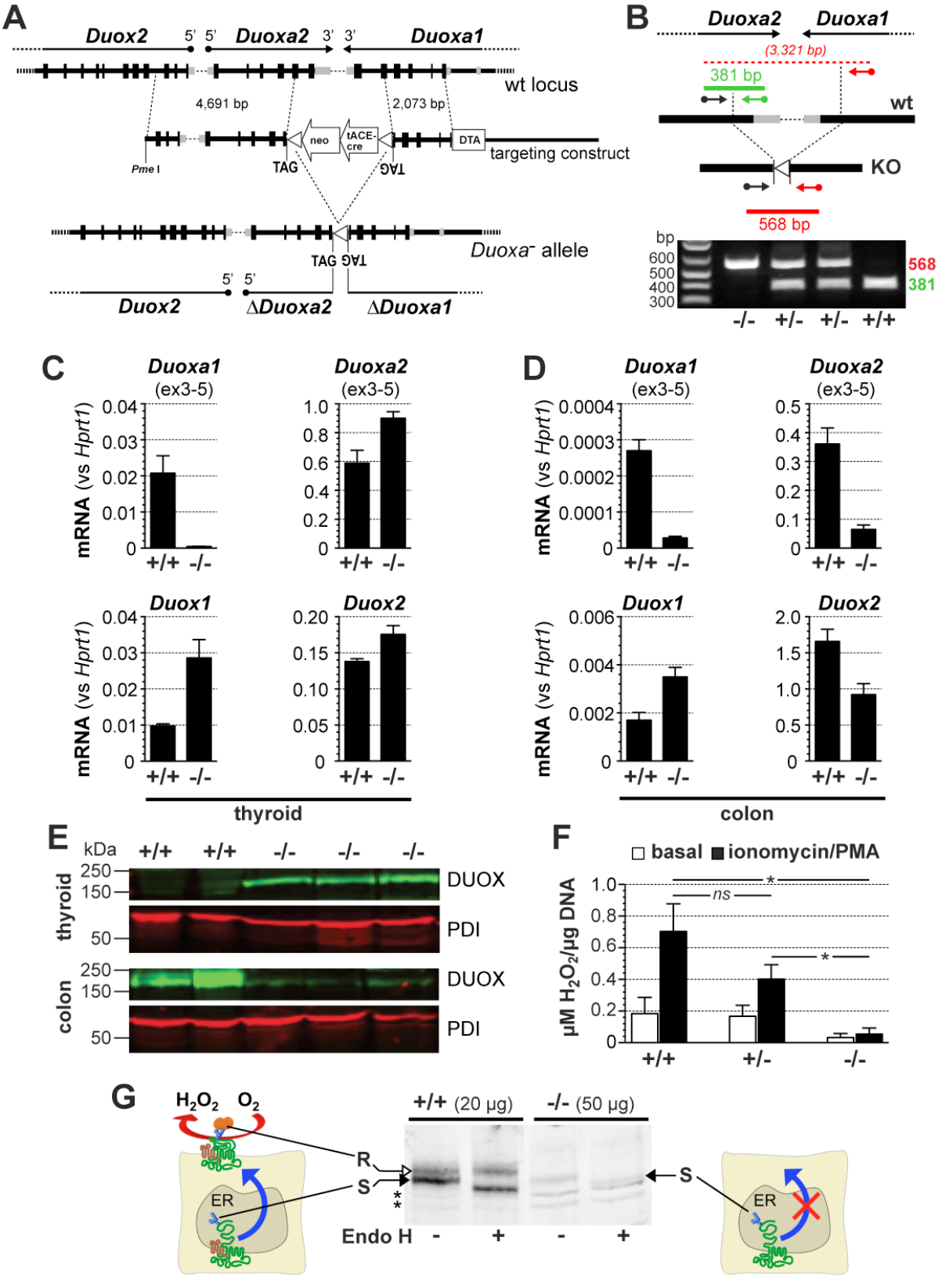
A
Duox2
Duoxa2
Duoxa1
wt locus
4,691 bp
2,073 bp
neo
tACE-cre
DTA
targeting construct
Pme I
TAG
Duoxa- allele
Duox2
ΔDuoxa2
ΔDuoxa1
B
(3,321 bp)
381 bp
wt
KO
568 bp
bp
600
500
400
300
568
381
-/- +/- +/- +/+
C
Duoxa1 (ex3-5)
Duoxa2 (ex3-5)
Duox1
Duox2
mRNA (vs Hprt1)
+/+ -/-
thyroid
D
colon
E
kDa +/+ +/+ -/- -/- -/-
thyroid
colon
250
150
50
DUOX
PDI
F
basal ionomycin/PMA
μM H2O2/μg DNA
ns
+/+ +/- -/-
G
H2O2 O2
ER
R
S
+/+ (20 μg)
-/- (50 μg)
Endo H - + - +

figure 1

660

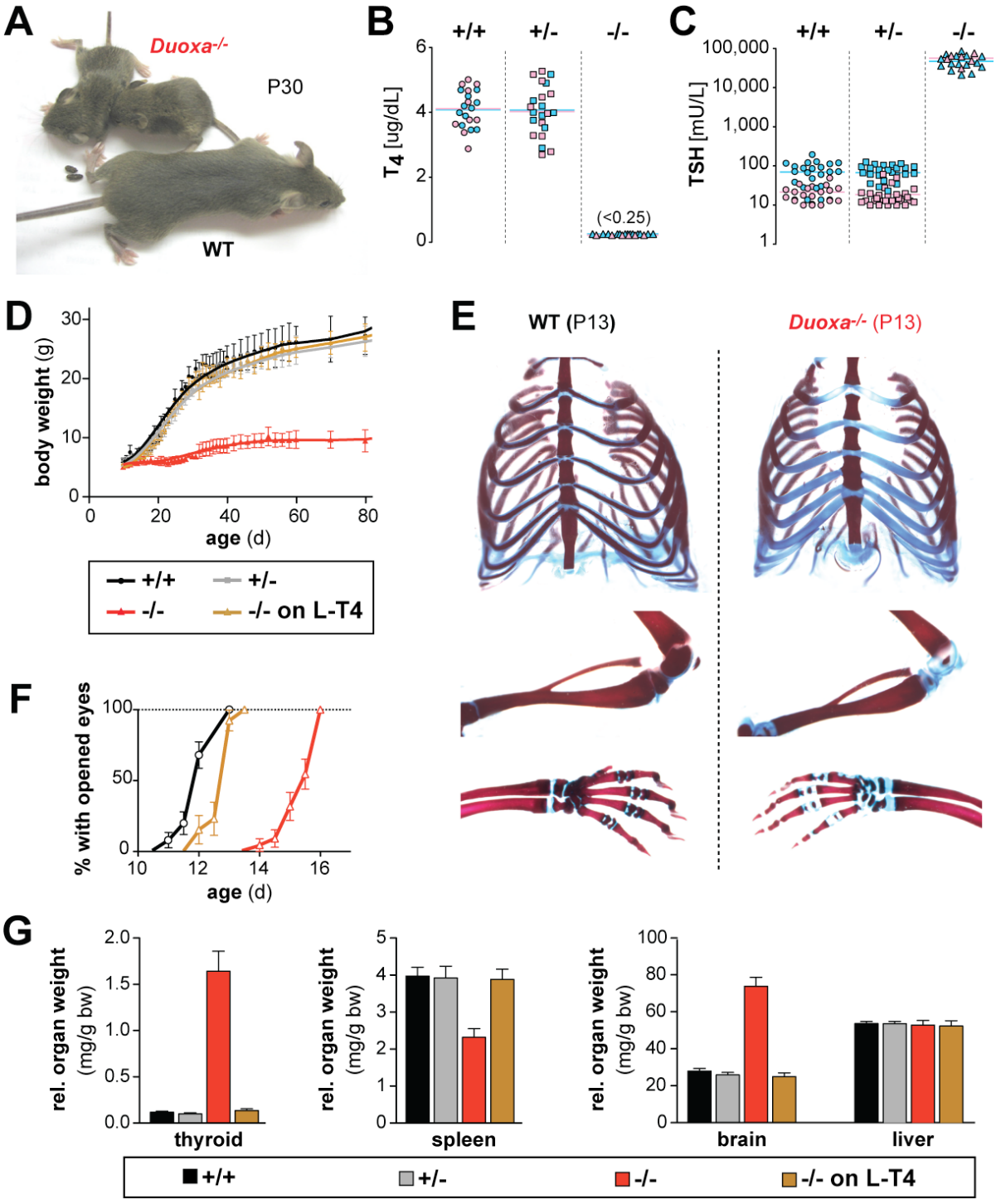
A
Duoxa-/-
P30
WT
B
+/+
+/-
-/-
T4 [ug/dL]
(<0.25)
C
TSH [mU/L]
D
body weight (g)
age (d)
+/+
+/-
-/-
-/- on L-T4
E
WT (P13)
Duoxa-/- (P13)
F
% with opened eyes
age (d)
G
rel. organ weight (mg/g bw)
thyroid
spleen
brain
liver
+/+
+/-
-/-
-/- on L-T4

figure 2

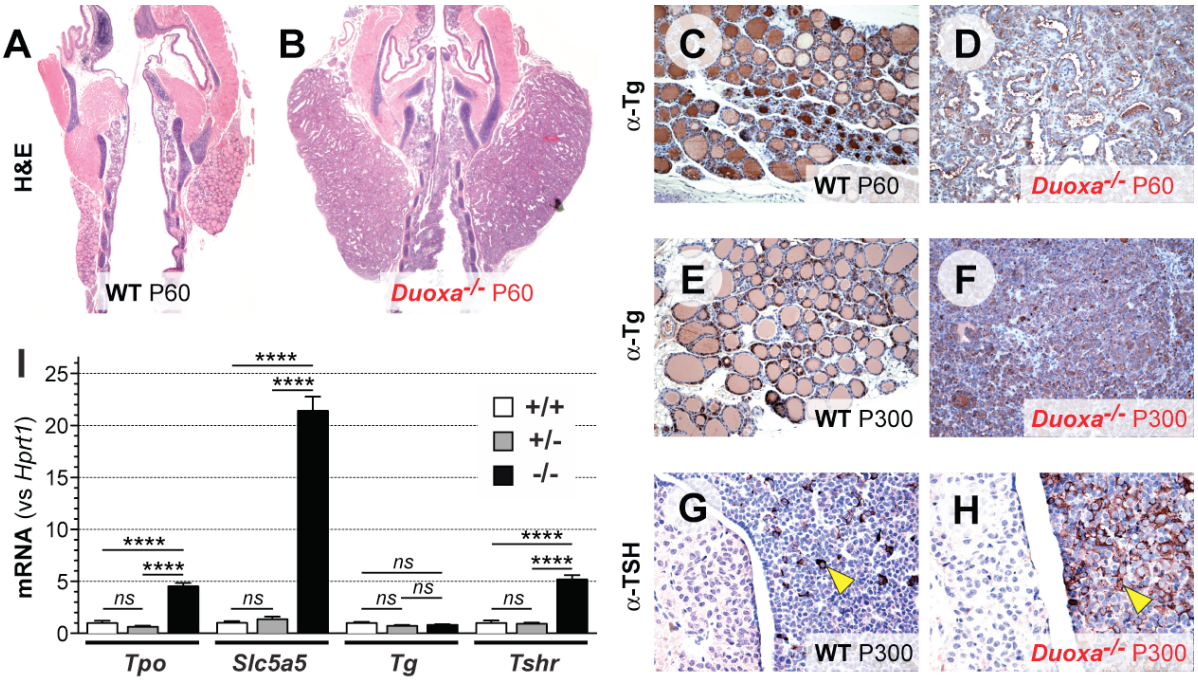
A
B
H&E
WT P60
Duoxa-/- P60
C
D
α-Tg
WT P60
Duoxa-/- P60
E
F
α-Tg
WT P300
Duoxa-/- P300
G
H
α-TSH
WT P300
Duoxa-/- P300
I
mRNA (vs Hprt1)
25
20
15
10
5
0
+/+
+/-
-/-
****
****
****
****
****
ns
ns
ns
ns
ns
ns
Tpo
Slc5a5
Tg
Tshr

figure 3

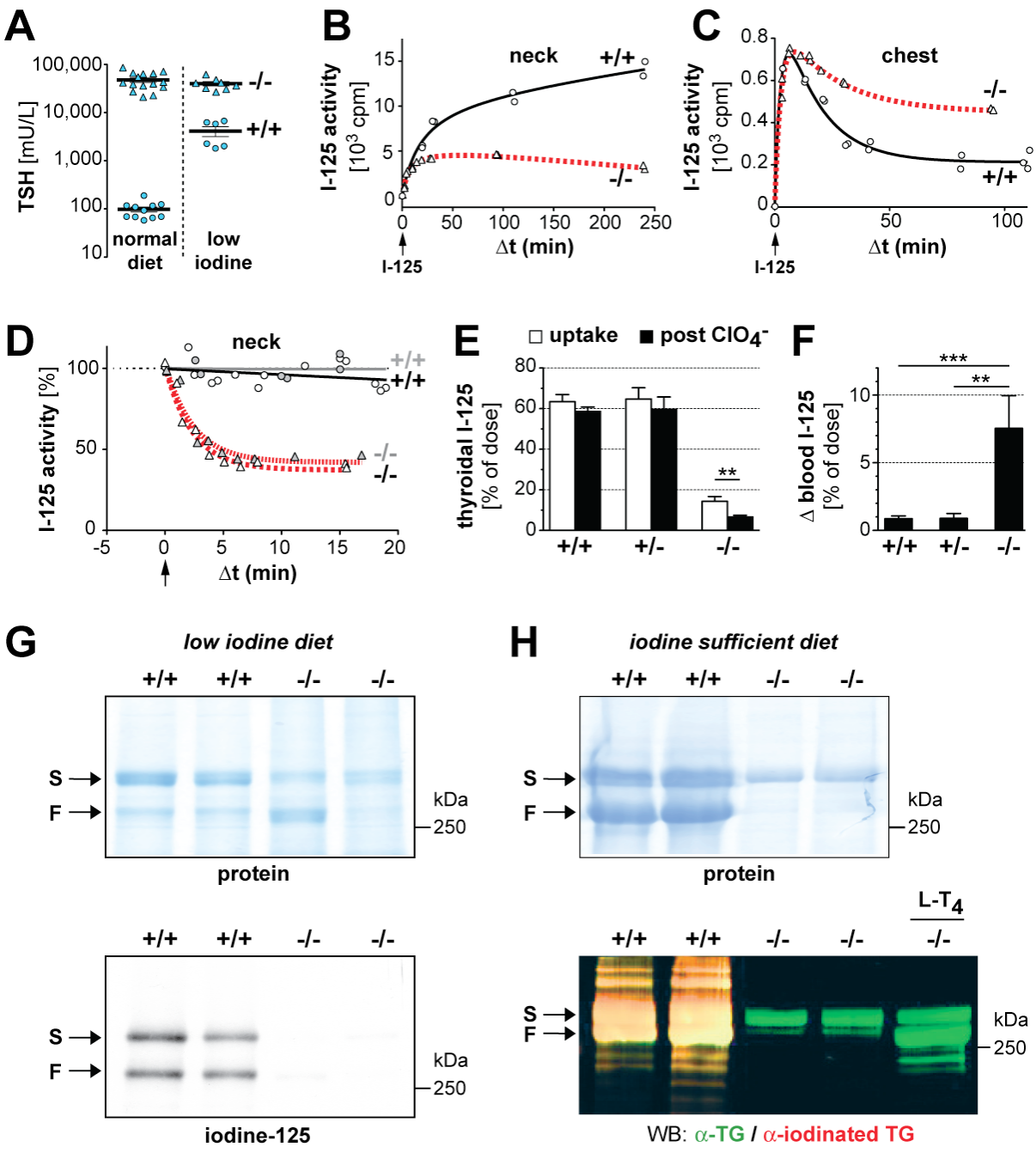
A
TSH [mU/L]
100,000
10,000
1,000
100
10
normal diet
low iodine
-/-
+/+
B
neck
I-125 activity [10³ cpm]
+/+
-/-
Δt (min)
I-125
C
chest
I-125 activity [10³ cpm]
-/-
+/+
Δt (min)
I-125
D
neck
I-125 activity [%]
+/+
-/-
Δt (min)
E
uptake
post ClO4-
thyroidal I-125 [% of dose]
+/+
+/-
-/-
F
Δ blood I-125 [% of dose]
***
**
G
low iodine diet
+/+ +/+ -/- -/-
S
F
kDa
250
protein
iodine-125
H
iodine sufficient diet
L-T4
WB: α-TG / α-iodinated TG

figure 4

670

671

672 **LEGENDS FOR SUPPLEMENTAL FIGURES**

673

674 **FIG. S1.** Screening of ES-cells for correct homologous recombination with the targeting construct. A)
675 Long range PCR was performed with Herculase II fusion DNA polymerase (Agilent Technologies) and
676 primers 5'-CCACACTCACCAGGTCTGA-3' and 5'-GGACACTACTCTGGCTGTCA-3', both outside
677 the region covered by the targeting construct (between the dashed lines). Amplicons from the WT allele
678 are cleaved by endonuclease *Dra*I into 6.3 kb and 3.6 kb fragments, whereas the targeted allele remains
679 uncut (10.9 kb). Results shown are representative for WT (+/+) and correctly targeted (+/-) ES cell clones.
680 B) Southern blot of *Dra*I-digested genomic DNA to confirm correct homologous recombination of the
681 long arm of the targeting construct. The 690 bp DNA template to generate a 32P-labeled probe by random
682 priming was amplified from isogenic DNA using primers 5'-CTTGGTAGATTGTGTGAGCACCT-3'
683 and 5'-GTGAGTGGGCTTGGAGCT-3'. Results shown are representative for WT (+/+) and correctly
684 targeted (+/-) ES cell clones.

685

686 **FIG. S2.** Schematic showing the sequence (in red) of stable, polyadenylated transcripts expressed from
687 the truncated *Duoxa2* locus (Δ*Duoxa2*). Transcripts were cloned by rapid amplification of 3' cDNA ends
688 (3'-RACE) using reagents from the GeneRacer system (Invitrogen) and gene specific primers 5'-
689 CTCGAACTTCTTGCAGGATGACT-3' (first-round amplification) and 5'-
690 CGTTAACATTACACTCCGAGGAACA-3' (nested PCR).

691

692

693

694

695

696 **TABLE S1:** List of primers used for real-time RT-PCR.

gene	forward (5'-3')	reverse (5'-3')
Duoxa1	CATCACCCTCACAGGCACC	GGAATGCCACCCACAGCA
Duoxa2	CGTTAACATTACACTCCGAGGAACA	CAGAATGCCACCCACAGTGT
Duox1	GGATGAGTTCATTAGGATGCTAAGGT	CTTCCGGCACTTCCACACCT
Duox2	GAGTTCTTCACCATGATGCGGT	CCTCCAGCTCCACCTTTGA
Polr2A	GTGGAGATCTTCACGGTACTG	CTTCCATAAGGACATCCACCGT
Tshr	GGACCAACTTTGCTAGATGTGTCT	GGTTCCGGATACTGCTCTCA
Tpo	GCAGGTGGACACATGCTGA	GTCTGGCTCCAAAGCAGTGA
Tg	CGTGGAAATGTCTTCATGTACCA	GTGGCAAACTCAGCTGCCT
Slc5a5	GGTGCTCTCATCAGCTACCT	GTCGCAGCAGGGATGTCT

697

698

699

700

701

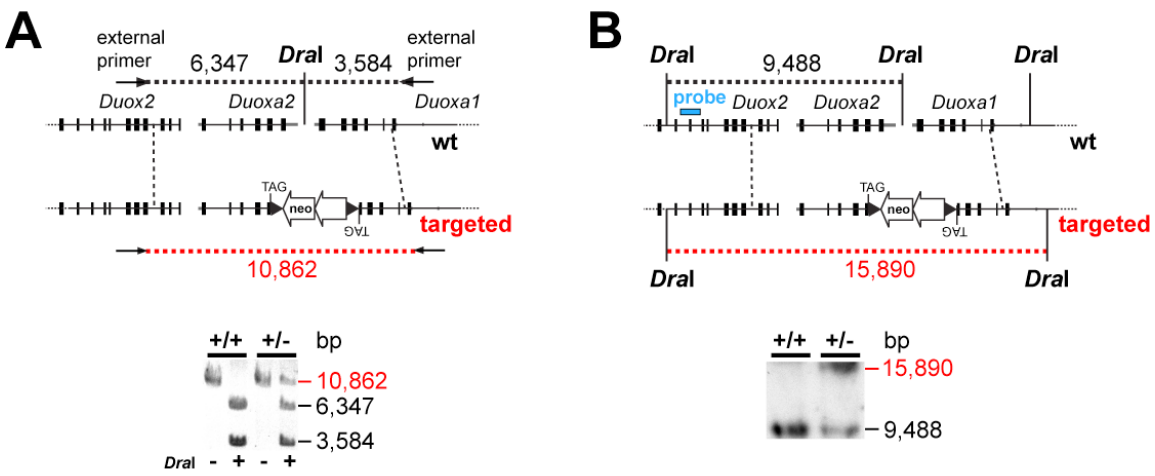

figure S1

3'-RACE product for *Duoxa2* in *Duoxa*$^{-/-}$ mice (in red)

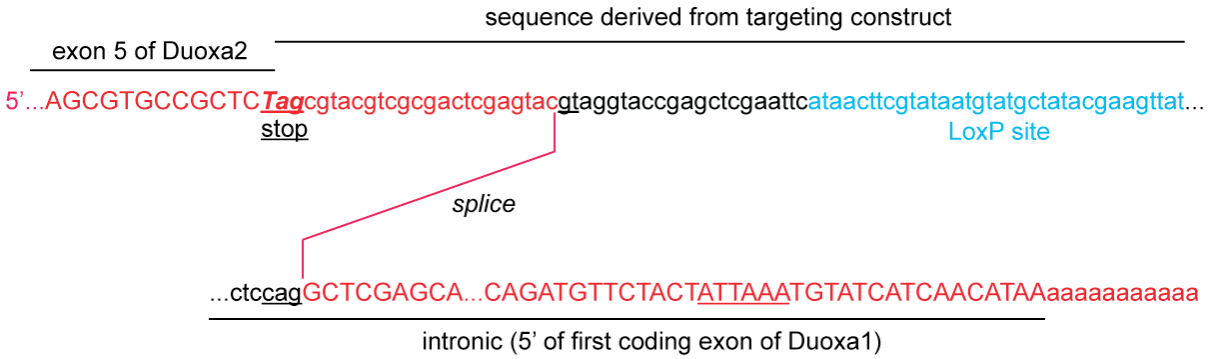

figure S2